Electron scattering from H_2O: Elastic scattering

M. A. Khakoo,[1] H. Silva,[2] J. Muse,[1] M. C. A. Lopes,[2] C. Winstead,[3] and V. McKoy[3]
[1]*Department of Physics, California State University, Fullerton, California 92831, USA*
[2]*Departamento de Física, ICE, Universidade Federal de Juiz de Fora, Juiz de Fora-MG, CEP 36036-330, Brazil*
[3]*A. A. Noyes Laboratory of Chemical Physics, California Institute of Technology, Pasadena, California 91125, USA*
(Received 18 September 2008; published 19 November 2008)

Differential cross sections for elastic electron scattering from gaseous water are reported. The measurements are obtained using the relative flow method with He as the standard gas and a thin collimating aperture source of gas instead of a conventional needle source. Differential cross sections were measured at incident energies of 1, 2, 4, 6, 8, 10, 15, 20, 30, 50, and 100 eV for scattering angles ranging from 5° to 130° and integrated over angles to obtain integral cross sections. Corresponding calculations of the differential cross section are carried out using the Schwinger multichannel method, employing extensive basis sets and considering polarization and dipole-scattering effects. Whereas excellent qualitative agreement with past measurements of differential cross sections is observed, our measurements are found to be consistently in significant quantitative disagreement with these measurements. The present calculations, on the other hand, generally agree in magnitude with previous results.

DOI: 10.1103/PhysRevA.78.052710 PACS number(s): 34.80.Bm

I. INTRODUCTION

Water plays a major role in life on Earth and is the third most abundant molecule in the universe after H_2 and CO. It also is important as a greenhouse gas [1] and in the dynamics of the troposphere, where much of our terrestrial water vapor lies. Among electron-water interactions, elastic scattering is a dominant process at energies below 100 eV [1]. In-depth modeling of electron transport in water or water-containing media (including living tissue) requires accurate elastic and inelastic cross sections, both integral and differential. Such modeling has been initiated by Pimblott and Siebbeles [2].

In view of their importance, much effort has been aimed at measuring the electron cross sections for water vapor. Elastic, inelastic, and total cross sections have been measured by several groups. A summary of this work is given in the recent and comprehensive review of Itikawa and Mason [1]; here, we mention only some relevant experiments. All total cross-section (TCS) measurements have been based on the Beer-Lambert law (see, e.g., Ref. [3]). Sueoka *et al.* [4] measured the TCSs for both positrons and electrons from 1 to 400 eV using a long scattering chamber (69.2 cm) incorporated into a time-of-flight system. In the linear transmission arrangement of Szmytkowski [3], a steady, highly collimated electron beam traverses a short gas cell (3.05 cm); this system is restricted to low incident energies, 0.5–80 eV. In both experiments, the difficulty of discriminating between unscattered electrons and electrons elastically scattered in the near-forward direction by the strong dipole of H_2O introduces uncertainty. Indeed, Kimura *et al.* [5] substantially revised the results of Sueoka *et al.* to correct for elastically forward-scattered electrons (see also [1]). The revised values of Kimura *et al.* greatly exceed all other experimental TCSs below 10 eV. Transmission setups similar to that used by Szmytkowski [3] were employed by Sağlam and Aktekin [6] and Nishimura and Yano [7], who obtain good agreement with the results of Szmytkowski [3]. The instrument of the Trento group [8] is of the well-known Ramsauer type, designed for intermediate-energy TCS measurements. Szmytkowski and co-workers have repeated their linear transmission measurements with different setups for H_2O [9] for energies from 0.5 to 370 eV and for D_2O [10] for energies from 0.4 to 100 eV in collaboration with the Trento group, who extended their measurements from 81 to 2707 eV, with very good overlap in the 81–100 eV region. The D_2O experiments were undertaken with the aim of detecting any isotopic effects due to different rotational population distributions. No significant effect was observed above 1 eV; however, below 1 eV "intriguing" [10] differences between the results of [3,10] could be observed, with the D_2O TCSs exceeding those for H_2O by as much as 16%, just outside the error bars.

Angle-differential elastic electron scattering from H_2O was studied as early as 1974 by Seng and Linder [11], who measured the relative cross section at a fixed angle of 90°. Differential cross sections (DCSs) at multiple angles were generated as early as 1982 by Jung *et al.* [12] and have since been measured by numerous groups [13–18]. The measurements of Seng and Linder [11] are relative, but the others were made absolute through normalization. All these measurements, except those of Katase *et al.* [14], used tube collimating sources for their target beam generation and invoked the conventional relative flow [19] to normalize the DCSs by comparison with a test gas, Ar or Ne in the case of Jung *et al.* [12] and He in all other cases. Katase *et al.* [14] measured relative DCSs from 100 to 1000 eV using a gas cell target and normalized their results to He. Katase *et al.* also calculated DCSs using two model potentials. The most recent DCS measurements, by Cho *et al.* [18], cover essentially the entire range of scattering angle (θ) from 10° to 180° using a magnetic angle-changer (MAC) device [20]. These various DCS measurements [12–18] are in very good qualitative agreement with each other, but significant quantitative disagreements exist among them. In addition, when angle integrated, they yield integral cross sections (ICSs) that are significantly smaller than the measured TCSs even at low

energy, reflecting the difficulty of integrating the dipole-induced forward peak in the DCS.

Early calculations of low-energy elastic electron scattering from H_2O were carried out by Gianturco and Thompson [21] using a local polarization potential and treating exchange through orthogonalization and by Jain and Thompson [22] employing local exchange and polarization potentials. More recent calculations include those by Brescansin *et al.* [23] using the Schwinger multichannel (SMC) method in the static-exchange approximation (i.e., neglecting polarization); by Gianturco and Scialla [24] using local exchange and polarization potentials; by Rescigno and Lengsfield [25] using the complex-Kohn method and a first-principles treatment of polarization; by Okamoto *et al.* in a local-potential formulation [26]; by Greer and Thompson using exact exchange and local polarization within a single-center expansion formalism [27]; by Machado *et al.* using the iterative Schwinger method in the static-exchange approximation [28]; by Gianturco *et al.* using exact exchange, local polarization, and explicitly considering rotation within the adiabatic approximation [29]; and by Varella *et al.* [30] and Natalense *et al.* [31] using the Schwinger multichannel method with pseudopotentials (SMCPP) in the static-exchange approximation. Recently, multicenter scattering was studied by Aouchiche *et al.* [32] for both gaseous and liquid H_2O using a local-potential formulation, while progress toward extending high-level scattering calculations into the condensed phase was discussed by Caron *et al.* [33] and Bouchiha *et al.* [34]. Muñoz *et al.* [35] reported stopping powers for electrons (E_0 from 50 eV to 5 keV) and recommended total scattering cross sections from 7.5 eV to 10 keV. Incorporating available inelastic and elastic cross sections into a Monte Carlo algorithm, Muñoz *et al.* [36] also reported a cross-section set developed from their own and literature data and used that set for Monte Carlo simulation of single-electron tracks in 500 mTorr of water vapor as a step toward simulation of radiation damage in living tissues. The most recent and sophisticated gas-phase calculations of the (vibronically) elastic cross section are those of Faure *et al.* [37,38], who used the *R*-matrix approach with a correlated wave function and computed rotationally resolved cross sections within the adiabatic approximation. At 4 and 6 eV, where comparison is possible, the rotationally summed DCSs of Faure *et al.* agree well with the measurements of Cho *et al.* [18] from 20° to 180°, but yield a substantially larger elastic ICS when integrated [37].

In this paper, we report calculated and experimental DCSs for elastic electron scattering from H_2O. We recently initiated a program of elastic electron-scattering measurements from polyatomic molecules using an improvement in the "conventional" relative flow method [19] wherein the conventional collimating tube gas source is replaced with a thin aperture. In this way, we remove the dependence of the gas source collimation on the gas-kinetic molecular diameter of either H_2O or the test gas (He). We measured DCSs for collision energies E_0 of 1, 2, 4, 6, 8, 10, 15, 20, 30, 50, and 100 eV for θ ranging from 5° to 130°. These measurements were normalized to helium elastic DCSs. The calculations use the Schwinger multichannel method [39] within an extensive one-electron basis set. Polarization effects are included, and a correction for long-range scattering by the dipole potential is applied to improve the accuracy of the forward DCS and the ICS. We compare our results with each other as well as with existing experimental and calculated DCSs for H_2O. We also compare our derived ICSs to each other and to existing ICSs and TCSs. We note here that a Letter with a subset of our experimental DCSs was published previously [40].

II. METHOD

A. Experiment

The experimental setup uses a modification of the "conventional" relative flow method that was first implemented by Srivastava *et al.* [19] and has been discussed in more detail elsewhere—e.g., in Brunger and Buckman [41]. Our innovation is to use a thin aperture source of gas instead of a tube collimator, so that one does not need to know the molecular diameters of the gases (see, e.g., [42–44]). In the relative flow method, which has been the only method available to date to enable measurement of DCSs, the DCS for scattering of the unknown gas is determined by comparing scattering signals from a standard target (usually helium gas) with that of an unknown gas under identical collision region geometry conditions while monitoring the gas flow rate of both target gases. Identical geometry conditions require that the electron beam profile, the electron detector profile, and the target gas beam profile at the electron-gas collision region be the same for both the standard gas and the unknown gas. To maintain the same profiles for both target beams when using a tube collimating source, the two gases must be operated at tube drive pressures that produce the same mean free paths [41]. For a thin aperture source, on the other hand, the profile of the gas beam is independent of the gas pressure, provided the mean free path (roughly and conservatively estimated) of the gas is greater than the thickness of the aperture (a condition that easily provides operation over a range of gas pressures behind the source). Our present gas-handling setup and implementation are described in detail in [42]. However, there are some important differences regarding the handling of H_2O in our experiment; notably, the gas-handling tubing (copper) in our system was heated to a constant temperature of 74 °C to ensure that the water did not condense on the tubing. The gas-handling tubing in the vacuum chamber was made of Teflon, and this was heated to a temperature of 90 °C. Repeated flow rate measurements during the course of this experiment revealed that the relative flow rate did not change by more than 2% for a given drive pressure setting. The temperature remained constant to within ±2 °C. The water was doubly distilled and placed in a vacuum flask that was sealed with an O-ring to the gas-handling system. The water was freeze pumped and thawed repeatedly (about 6 times or more) to remove dissolved gases. Measurements of the relative flow rate $\dot{N}_R$, which is directly proportional to the flow rate of gas through the system, $\dot{N}$, as a function of drive pressure P_s were made by filling a closed volume and determining the (linear) rate of rise of pressure in the gas-handling line, as measured by a

TABLE I. Experimental a and ε coefficients determined from $\dot{N}_R$ measurements in our experiment at different values of T for several gaseous (upper section) and vapor targets (lower section). The correction factor ξ [according to Eqs. (1a) and (1b)] can be either expressed via a direct relation with the system geometry ($=DA/L$) or an inverse $\sqrt{M}$ relation. The value of ξ for gaseous targets is 1 since these directly obey Eqs. (1a) and (1b), to give an average relative $a\sqrt{M}$ (relative $\mathrm{kg^2\,m^2\,s^{-2}}$) of 0.313 ± 0.009 (a factor dependent on the gas handling system's physical dimensions). However, the vapors do not obey Eqs. (1a) and (1b) and a has to be corrected. See text for discussion of corrections used.

Gas	T (°C)	a ($\mathrm{s^{-1}}$)	ε ($\mathrm{Torr^{-1}}$)	δ (10^{-8} cm)	M	$a\sqrt{M}\xi$	ε/δ^2	$\xi=1/L_f$	$\xi=\sqrt{M_t}$
H_2	25	0.2181	1.050	2.74	2.016	0.310	1.40	1	1
He	25	0.1551	0.739	2.18	4.002	0.310	1.56	1	1
He	47	0.1611	0.638	2.18	4.002	0.322	1.34	1	1
He	74	0.1615	0.659	2.18	4.002	0.323	1.39	1	1
N_2	25	0.0596	2.115	3.75	28.02	0.316	1.50	1	1
C_2H_4	25	0.0566	4.070	4.95	28.02	0.300	1.66	1	1
H_2O	74	0.0242	7.792	7.25	18.02	0.313	1.48	0.33	9.25
H_2O	24	0.02544	6.943	7.00	18.02	0.313	1.42	0.34	8.41
CH_3OH	47	0.0387	5.722	6.30	32.04	0.313	1.44	0.70	2.04
CH_3OH	74	0.0475	4.614	5.67	32.04	0.313	1.44	0.86	1.36
C_2H_5OH	47	0.0352	7.346	7.15	46.07	0.313	1.44	0.76	1.72
C_2H_5OH	74	0.0373	6.508	6.73	46.07	0.313	1.44	0.81	1.53
C_3H_7OH	74	0.0288	8.095	7.49	60.11	0.313	1.44	0.71	1.96
C_4H_9OH	74	0.0212	9.754	8.23	74.12	0.313	1.44	0.58	2.94

capacitance manometer which was monitored by the experiment computer [42]. The resulting $\dot{N}_R$ vs P_s curve was fitted to a second-order polynomial in P_s with a high correlation coefficient (greater than 0.999). This second-order polynomial has some physical significance [43,44] because it can be expressed as

$$\dot{N} = \frac{\kappa\sqrt{N_A}A}{\sqrt{(2\pi MkT)}}P_s\left[1 + \frac{2\sqrt{\pi}\delta^2 D}{10\sqrt{2}kT}P_s\right] \tag{1a}$$

and can be simplified using two constants as

$$\dot{N} = aP_s[1 + \varepsilon P_s], \tag{1b}$$

where κ is the Clausing (geometrical transmission) factor for gas in the reservoir leaving the exit orifice of the system and is dependent on the geometry of the gas-handling system. For a straight tube of diameter D and length L of the gas-handling system and exit area A, κ equals $D/3L$ [43,44]. M is the molar mass of the gas, N_A is Avogadro's number, k is Boltzmann's constant, and T is the temperature of the gas. Thus for a fixed T, the linear part of Eq. (1a) and (1b) (constant a) depends only on the geometry of the gas-handling system, but the effect of the extra P_s term, (the nonlinearity constant ε), depends on the gas-kinetic molecular diameter squared δ^2 ($\approx$ the gas-kinetic molecular cross section). We have measured $\dot{N}_R$ for He, H_2O, and other gases and have normalized the coefficients for the linear and nonlinear parts to the molar mass of He and its δ^2 value, respectively. From this table we should be able to obtain the molar masses and δ^2 for the other gases from the a and ε coefficients. Table I shows the results for several gases and vapors. From Table I, we note that for regular gases, the a coefficient is inversely proportional to the square root of the molecular mass of the gas, while the ε term is proportional to δ^2, as expected. However, this is not the case for the vapors, and a has to be modified by a scaling factor ξ that can be interpreted as a change in some effective DA/L dimension of the gas handling system or as a change in the M value of the gas due to the production of multimers—e.g., for H_2O this would seem to imply the production of $(H_2O)_9$, which would be incorrect. The possible presence of dimers in low-pressure water vapor was investigated theoretically by Goldman *et al.* [45], who calculated the equilibrium constant for water dimerization using the most accurate water dimer potential energy surface. We have interpolated their partial fraction of $(H_2O)_2/H_2O$ as a function of pressure of H_2O and find that, at our P_s of 0.5 Torr for H_2O, the dimer fraction should be conservatively at most $<3\times10^{-3}$ and probably closer to 10^{-5}. Interestingly, Danjo and Nishimura [13] operated their multicapillary gas source of H_2O at a high pressure of 2 Torr, yet failed to detect the presence of $(H_2O)_2$ in their beam with a quadrupole mass spectrometer placed downstream of the gas source. While it could be that the ionization of $(H_2O)_2$ is dissociative and defeats this detection technique for dimers, their result is consistent with the results of [45]. This arguably suggests that the factor in a is due to DA/L—i.e., a decrease in D or A or an increase in L. An increase in L possibly indicates that the vapor is sticking to the sides of tubing and spending about 3 times longer in the tube (see ξ in Table I for H_2O). However, this does not affect the flow rate, which is determined by the gas bleed valve setting. To be sure we were not getting condensation in the gas bleed valves, these were also heated to 74 °C. Nonetheless, a definitive measurement of dimers in the beam should be made using a negative-ion-mass spectrometer, and we plan to do this in the near future.

Another feature of Table I is that the value of δ^2 may be determined from the nonlinear part of Eq. (1b)—viz., the ε term. From normalization we obtained the value of $(7.13 \pm 0.37) \times 10^{-8}$ cm for δ, which is significantly higher than that quoted by other workers (e.g., [15]), around 4.2×10^{-8} cm. This result was also discussed in our Letter [40] and may have ramifications for the DCSs measured for H_2O using relative flow with collimating tube sources, as discussed in the next section.

The possibility of gas condensation was checked by repeating measurements at different relative flow rates, and it was found that low-pressure flow rate measurements could be reproduced after high-pressure flow rate measurements and vice versa. However, it was observed that water did condense on the outer walls of the vacuum chamber, resulting in raised base pressures, normally 1×10^{-7} Torr to 1.5×10^{-7} Torr (our experimental pressure with gas running into the target region was in the range from 8×10^{-7} to 1.5×10^{-6} Torr). This pressure reverted back to normal base pressure within about 4–6 h of pumping. We also attempted to detect dimers in the beam by looking at forward-electron-scattering effects (see second paragraph following), without success.

Our experimental apparatus (spectrometer, vacuum chamber, control equipment) has been described in detail in previous papers—e.g., Khakoo *et al.* [46]—and only a brief description will be given here. The electron gun and the detector employed double-hemispherical energy selectors, and the apparatus was made of titanium. Cylindrical lenses were utilized, and the system was baked to about 130 °C with magnetically free biaxial heaters [47]. The analyzer detector was a discrete dynode electron multiplier [48] with extremely low background rate of <0.01 Hz and capable of linearly detecting $>10^5$ Hz without saturating. The remnant magnetic field in the collision region area was reduced to less than 1 mG by using a double μ-metal shield as well as a coil that eliminated the vertical component of the Earth's magnetic field. Typical electron currents were around 20 nA, with an energy resolution of 50–60 meV, full width at half maximum. The electron beam could be easily focused at 1 eV and remained stable, varying less than 10% at maximum, during the day's data taking. The energy of the beam was established by repetitively (at least daily) determining the dip in the elastic scattering of the $2\,^2S$ He^- resonance at 19.366 eV [49] to be stable to better than ± 10 meV during an experimental run (1 day). Typically the contact potential varied as the electron beam settled with time. This contact potential depends sensitively on the setting of the monochromator's double hemispheres combined with the extraction voltage setups near the filament and varies slowly on a daily basis. In our case, for a filament heater power supply voltage of approximately 4.3 V, and 2.2 A, our contact potential was typically 0.85 V (i.e., the electrons had a 0.85 eV kinetic energy for a lens operating at 0 V with respect to the filament). It varied during our experiments with H_2O from 0.75 to 0.95 V. (As an interesting note, it varies most significantly during the final days' lifetime of the filament—our case to nearly 1.5 V.) Energy loss spectra of the elastic peak were collected at fixed E_0 values and electron scattering angles θ by repetitive, multichannel-scaling techniques. The

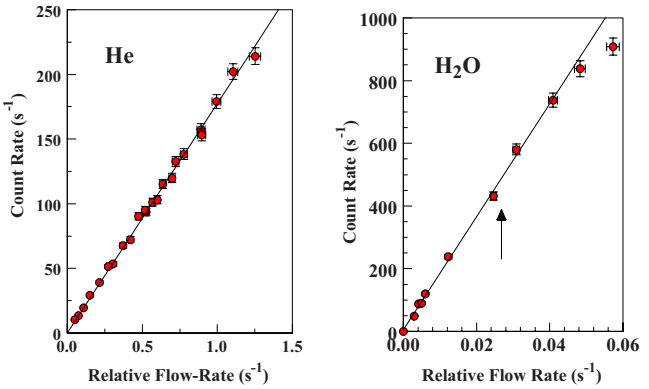

FIG. 1. (Color online) (●) Scattered electron signal rate (background corrected) vs gas flow rate for He and H_2O at $E_0=20$ eV and $\theta=30°$ and (solid line) linear fit to data. Note that while He displays a linear dependence, H_2O shows a nonlinear dependence at higher pressures. The arrow in the figure for H_2O is approximately the upper limit in flow rate region of operation of our experiment.

effusive target gas beam was formed by flowing gas through an aperture, which was constructed by mounting a thin disk of 0.025-mm-thick brass shim stock into a flush recess at the end of brass tube, with an outer diameter of 6.35 mm and an inner diameter of 4.3 mm, as an aperture source. The aperture (0.3 mm diameter) was punched into the shim stock with a straight sharp sewing needle, while the brass tube was rotating in the lathe (thus the aperture was located centrally and flush at the end of the tube), sooted to reduce secondary electrons, and placed 6 mm below the axis of the electron beam. The tube was incorporated into a moveable-source [50] arrangement. The moveable-gas-source method has already been well tested in our laboratory and determines background scattering rates expediently and accurately in electron scattering experiments.

Monitoring the energy position of the He^- $(2\,^2S)$ resonance, with the moveable gas source in and out of place, revealed a <0.03 V potential variation in the system. We also observed a small, yet noticeable ($\approx 3\%$ at $E_0=20$ eV and $\theta=30°$), deviation from linearity in the scattered signal versus relative flow rate at the high P_s end (see Fig. 1) of up to 5%, in contrast to the linear behavior observed in earlier tests with ethylene, N_2, H_2 [51], methanol, and ethanol [52]. The origin of this effect is unclear, but does not appear to be due to dimer formation: the deviation from the trend is negative, whereas the presence of the dimer, which has both a larger geometric cross section and a larger dipole moment than the monomer, should increase the scattered signal rather than decrease it.

Using the relative flow method, the elastic scattering DCS for water (DCS_{HOH}) can be related to the DCS for He to first order by the equation (see, e.g., [41])

$$DCS_{HOH}(E_0,\theta) = \frac{I_{e\ He}}{I_{e\ HOH}} \frac{\dot{N}_{R\ He}}{\dot{N}_{R\ HOH}} \frac{I_{s\ HOH}}{I_{s\ He}} \times \sqrt{\frac{M_{He}}{M_{HOH}}} DCS_{He}(E_0,\theta), \qquad (2)$$

involving the electron scattering rate I_s, relative flow rates $\dot{N}_R$

TABLE II. Coordinates (atomic units) of extra centers (X) used in the calculations. The coordinates of the H and O nuclei are given as reference points.

Center	z	y	z
H	±1.44226	1.0012	0
O	0	−0.12617	0
X	±1.44226	−1.25354	0
X	0	−2.0159	0
X	0	1.76356	0
X	±1.88973	−0.12617	0
X	±0.94486	−0.12617	±1.88973
X	0	−1.07103	±1.88973
X	0	0.81693	±1.88973
X	±2.26767	±0.94486	±1.88973
X	±2.26767	±2.26767	0
X	±3.77945	0	0
X	0	±3.77945	0

(s^{-1}), the incident electron beam currents (I_e), and the molecular masses (M), appropriately subscripted for helium and water. The DCSs for helium were taken from [53,54]. In our experiments, the electron current I_e did not vary by more than 10% for a run comprising the different gases, and measurements were repeated several times a day as well as over several days after retuning the electron beam. The DCSs were integrated over angle to obtain ICSs with the help of extrapolation to backward and forward angles.

B. Theory

The goal of the present calculations was to determine whether an extensive computational treatment of elastic scattering by water could account for discrepancies noted in a preliminary publication [40] between the present measured DCSs and earlier calculations. Accordingly, we attempted to account well for all relevant aspects of the collision physics, within the limitations of our computational procedures.

Calculations were carried out using the SMC method [39] as implemented for parallel computers [55], within the fixed-nuclei approximation. A description of the method may be found in the indicated references; here, we give only details specific to the present calculations. The H_2O nuclear geometry was optimized in the 6-31G(d) basis set as contained in the electronic structure package GAMESS [56] at the level of second-order Möller-Plesset perturbation theory, resulting in an HOH angle of 103.97° and an OH distance of 0.969 Å. A single-configuration Hartree-Fock ground-state wave function for H_2O was computed at this geometry in a basis set comprising the augmented correlation consistent polarized valence triple zeta (aug-cc-pVTZ) basis [57,58], with the f orbitals and most diffuse s orbital on O omitted and a d orbital on O (exponent 0.214) added, together with a $2s1p$ supplement of uncontracted Cartesian Gaussian orbitals located on each of the 30 extra centers listed in Table II. The exponents of these supplementary functions were 1.0 and 0.3 (s) and 0.388 (p). The virtual-orbital space from the Hartree-Fock calculation was used to construct the variational space of 11-electron doublet configuration-state functions (CSFs) describing the electron-molecule scattering system used in the SMC calculations. To accelerate convergence, an orthogonal transformation of the Hartree-Fock virtual orbitals into modified virtual orbitals (MVOs) [59] was performed using a +4 cationic Fock operator. All 227 CSFs formed by combining the neutral ground state with an MVO were included in the variational space. To describe polarization effects, we also included doublet CSFs formed by coupling any one of the MVOs to singlet or triplet singly excited configurations of the target molecule. The singlet-coupled space included excitations from all 4 valence occupied orbitals into the 20 lowest-energy MVOs, while the triplet-coupled space included excitations from the 3 outermost occupied orbitals into the 20 lowest MVOs. Separate scattering calculations were carried out for each irreducible representation of the C_{2v} point group. The variational space comprised 8211 A_1, 7100 A_2, 7389 B_1, and 7917 B_2 CSFs (where B_1 and B_2 are defined to be odd and even, respectively, on reflection in the plane of the nuclei).

Despite the inclusion of supplementary functions centered away from the nuclei, we do not expect the square-integrable basis set underlying the SMC calculations to describe well collision events at large impact parameter. For a strongly polar molecule such as water, such events make a large contribution to the total scattering cross section, owing to weak (near-forward) scattering by the long-range dipole potential. As is commonly done, we account for long-range scattering by applying a closure procedure based on the first Born approximation to scattering by a point dipole [60]. Details of our particular implementation of Born closure are given elsewhere [52]; however, an error in the overall sign of the Born amplitude has been corrected in the present work, and we have slightly extended the previous treatment to allow for specification of a small energy loss (inelasticity) that prevents divergence of the DCS at 0° and of the ICS. We used the dipole moment determined from our Hartree-Fock target wave function for H_2O, 1.9985 D, to determine the Born amplitude and retained exit-channel partial waves from the SMC calculation up to $\ell_{max}=1$ for collision energies of 1 and 2 eV, $\ell_{max}=2$ at 3 and 4 eV, $\ell_{max}=3$ at 5 and 6 eV, $\ell_{max}=4$ from 7 to 9 eV, $\ell_{max}=5$ from 10 to 14 eV, and $\ell_{max}=6$, 7, and 8 at 15, 20, and 30 eV, respectively.

III. RESULTS AND DISCUSSION

Our experimental DCSs are given in Table III and are plotted along with our calculated DCSs and literature values in Fig. 2. From the figure, we note generally good agreement between the shapes of the present measured and calculated DCSs; however, there are differences in magnitude at higher energies. On the other hand, very good agreement in shape and magnitude is found between the measured values and the pure Born-dipole approximation DCSs below $E_0=4$ eV. The Born-dipole DCSs shown in Fig. 2 were obtained [61] as

$$\text{DCS (elastic)} = \frac{4}{3}\mu^2\frac{k_f}{k_i}\frac{1}{K^2}, \tag{3}$$

where μ is the electric dipole moment of H_2O in a.u., k_f and k_i are the scattered and incident electron momenta (a.u.),

TABLE III. Experimental DCSs for vibrationally elastic scattering of electrons from H_2O with 1 standard deviation error bars. Data in italics are extrapolated DCSs. For small θ we supply the Born-dipole DCS results. Integral cross sections ICS* were obtained using the Born-dipole extrapolation of DCSs to small θ, where possible, and ICS# were obtained without the Born-dipole extrapolation. DCSs are in 10^{-16} cm^2/sr units whereas ICSs are in 10^{-16} cm^2 units. See text for discussion.

E_g (eV) →	1		2		4		6		8		10		15		20		30		50		100	
θ (deg) ↓	DCS	Error	DCS	Error	DCS	Error	DCS	Error	DCS	Error	DCS	Error	DCS	Error	DCS	Error	DCS	Error	DCS	Error	DCS	Error
0	*506051*		*1014440*		*2031217*		*3047995*		*4064773*		*5081551*		*7623495*		*101654*							
5	*363*		*177*		*88.3*		*58.9*		*44.2*		*35.3*		*23.6*		*20*		31.1	4.7	31.3	6.2	14.8	2.1
10	*58.5*		*44.3*		*22.1*	6.6	18.5	2.2	18.2	2.2	14.4	2.4	11.0	1.6	14.5	2.1	15.5	2.5	13.1	1.9	9.66	1.26
15	27.4	5.4	20.1	5.1	11.8	2.0	9.73	1.19	9.98	1.28	9.51	1.43	7.64	1.08	9.83	1.33	*10.00*		*7.80*		5.00	
20	18.0	1.9	11.2	2.2	7.17	1.43	6.54	0.87	6.98	0.97	6.94	0.95	5.88	0.75	6.93	0.85	6.77	0.82	5.05	0.704	2.675	0.351
30	9.00	1.24	5.13	0.92	3.75	0.62	3.53	0.42	3.84	0.51	3.94	0.48	3.69	0.51	3.96	0.51	3.27	0.42	1.96	0.240	0.817	0.102
40	5.72	0.66	2.90	0.52	2.22	0.36	2.20	0.25	2.49	0.32	2.57	0.32	2.33	0.29	2.1	0.26	1.69	0.21	0.91	0.117	0.353	0.041
50	3.48	0.44	1.77	0.30	1.47	0.25	1.58	0.21	1.74	0.21	1.87	0.23	1.62	0.19	1.25	0.14	0.94	0.11	0.46	0.063	0.191	0.025
70	1.76	0.20	0.867	0.176	0.884	0.147	1.12	0.14	1.23	0.15	1.19	0.15	0.814	0.101	0.573	0.087	0.390	0.048	0.197	0.023	0.075	0.010
90	1.20	0.15	0.537	0.0066	0.616	0.093	0.873	0.113	0.980	0.121	0.940	0.116	0.621	0.074	0.382	0.052	0.249	0.032	0.101	0.012	0.044	0.005
110	1.05	0.12	0.383	0.062	0.397	0.058	0.589	0.073	0.670	0.064	0.673	0.083	0.491	0.057	0.332	0.043	0.227	0.029	0.112	0.015	0.066	0.009
130	1.03	0.18	0.371	0.065	0.360	0.063	0.585	0.089	0.737	0.096	0.821	0.107	0.739	0.094	0.547	0.068	0.430	0.054	0.288	0.037	0.130	0.016
140	*1.1*		*0.4*		*0.4*		*0.6*		*0.8*		*0.9*		*0.9*		*0.8*		*0.48*		*0.37*		*0.166*	
150	*1.2*		*0.45*		*0.4*		*0.65*		*0.85*		*0.98*		*1.1*		*1.1*		*0.60*		*0.38*		*0.20*	
160	*1.25*		*0.5*		*0.4*		*0.7*		*0.9*		*1.1*		*1.4*		*1.5*		*0.69*		*0.42*		*0.26*	
170	*1.3*		*0.6*		*0.5*		*0.75*		*0.95*		*1.2*		*1.7*		*2*		*0.77*		*0.48*		*0.30*	
180	*1.4*		*0.7*		*0.6*		*0.8*		*1*		*1.4*		*2*		*2.5*		*0.87*		*0.55*		*0.35*	
ICS*	94.2	34.7	48.3	14.3	29.4	4.6	26.3	4.5	25.9	3.6	24.9	3.5	19.8	2.7	17.9	2.5						
ICS#	40.3	6.0	24.3	3.6	19.4	2.9	18.9	2.8	20.9	3.1	20.8	3.1	17.2	2.6	16.4	2.5	13.9	2.1	8.57	1.44	5.02	0.75

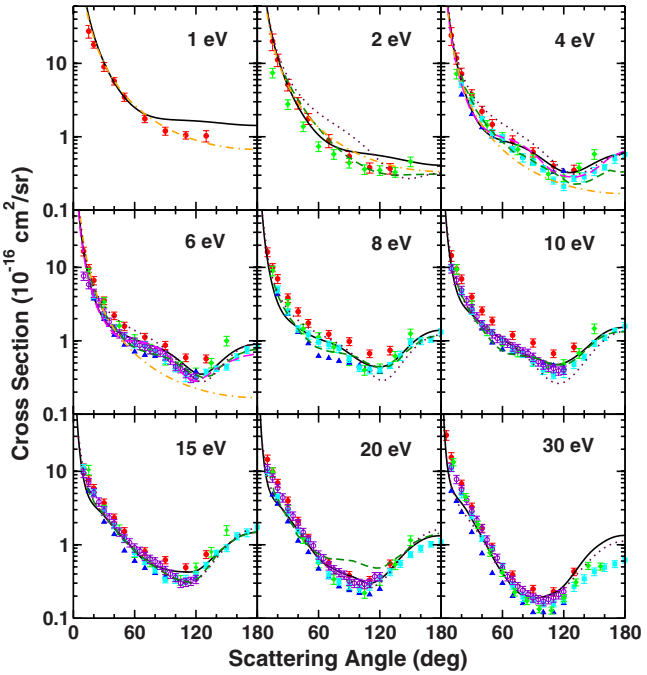

FIG. 2. (Color online) Elastic electron scattering DCSs for H_2O at various E_0. Experiments: (●) (red), present experiment, (▲) (blue), Danjo and Nishimura [13]; (♦) (green), Shyn and Cho [15] up to 20 eV (2.2 eV data shown at 2 eV) and Shyn and Grafe [17] at 30 eV; (○) (violet), Johnstone and Newell [16]; ■ (cyan), Cho *et al.* [18]. Calculations: solid line (black), present; short dashed line (short green dashes), Rescigno and Lengsfield [25]; dotted line (maroon dots), Varella *et al.* [30,31]; long dashed line (long magenta dashes), Faure *et al.*, rotationally summed DCS at E_0=4 eV [37] and E_0=6 eV [38]; and dot-dashed line (orange chain curve), Born-dipole approximation. See text for discussion.

and K^2 is the momentum transfer squared ($=k_f^2+k_i^2-2\,k_f k_i \cos\theta$). For water μ is 0.730 a.u. [62]. To prevent the Born-dipole DCSs from becoming infinite at $\theta=0°$, we used the 4.6 meV energy loss of the $J=0_{00}\rightarrow 1_{11}$ rotational transition [63] in computing k_f. The pure Born-dipole approximation rapidly loses validity at larger θ as E_0 increases; at E_0=6 eV, it works well only below $\theta=15°$, whereas the range of validity at E_0=1 eV extends up to 130°.

Comparison with past experiments shows that our measured results are from 30% to 50% larger than other measurements. However, agreement in shape with other experiments is excellent, especially with the results of Cho *et al.* [18], which if scaled up agree in most cases with our values across the whole angular range, within error bars, except at their highest E_0 of 50 eV, where significant agreement in shape can still be observed. The work of Cho *et al.* is significant because they cover the entire backward scattering region by using a MAC device, providing information useful in scaled extrapolation of our DCSs to backward-scattering angles to determine ICSs. At intermediate energies, around 20 eV, best agreement is observed between our measurements and those of Johnstone and Newell [16].

The present calculated DCSs agree quite closely with the rotationally summed results of Faure *et al.* [37,38] at 4 and 6 eV and are also close to the results calculated by Rescigno and Lengsfield [25] and by Varella and co-workers [30,31] at most energies and angles. Moreover, they generally agree well in shape and magnitude with the measurements of Cho *et al.* [18], although the present results are more strongly backward peaked at 20 and especially 30 eV.

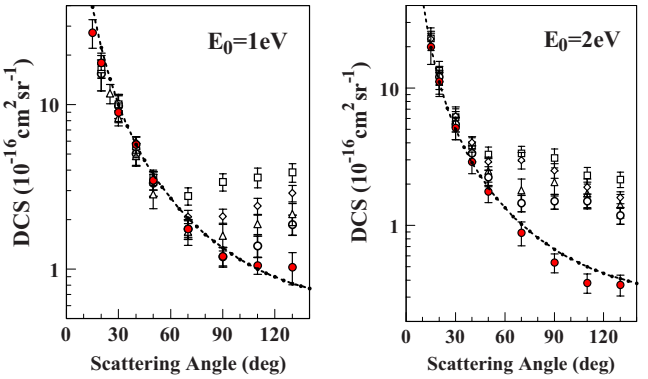

FIG. 3. (Color online) Experimental elastic electron scattering DCSs for H_2O at E_0=1 eV and 2 eV. Legend: Experiments (●) (red) H_2O. Present results; (○) (black) methanol and (△) ethanol [52], (◇) (black) propanol and (□) butanol, unpublished, in progress [64]. Theory: (-----) Born-dipole approximation for H_2O. See text for discussion.

Figure 3 shows our measured DCSs for H_2O at 1 and 2 eV together with DCSs from earlier [52] and ongoing [64] work for primary normal alcohols and with the Born-dipole approximation DCS for H_2O. The dipole moments of the alcohols (0.669, 0.665, 0.661, and 0.653 a.u. for methanol, ethanol, *n*-propanol, and *n*-butanol, respectively [65]) are close to that of H_2O (0.730 a.u.) [62]. Clearly dipole scattering dominates for θ less than 40° at the E_0 values displayed in these figures. We also observe that the backward-scattering DCSs are governed by the molecular size, with butanol largest and methanol smallest among the alcohols and water yet smaller. At E_0=1 eV the DCS for H_2O follows the Born-dipole DCS over $\theta>90°$, while the other molecules depart from the Born-dipole curve essentially in order of their size, likely reflecting the increased importance of non-dipolar scattering of low partial waves as the size of the target grows.

In Fig. 4, we show ICSs derived from the present results. We note here that in our earlier report of our experimental measurements [40], our ICSs were determined using a visual extrapolation of our DCSs at larger and smaller scattering angles. However, here we employed the Born-dipole expression of Eq. (3), with the $J=0_{00}\rightarrow 1_{11}$ energy loss of 4.6 meV, to extrapolate our measured DCSs at small θ in order to determine the ICS for E_0 below 30 eV, since we have been made aware of the significant small-angle contribution of the ICS due to the extreme forward-scattering nature of dipole scattering in the Born-dipole approximation. Assuming a larger energy loss would produce a smaller ICS; with 10 meV inelasticity, for example, the ICS would be reduced by ≈10% at 1 eV and by ≈1% at 20 eV. Where possible, for $\theta>130°$, we have used the DCSs of Cho *et al.* [18], which are in excellent qualitative agreement with our DCSs up to E_0=30 eV, to extrapolate our measured DCSs to 180°. Otherwise, we have used visually extrapolated DCSs for

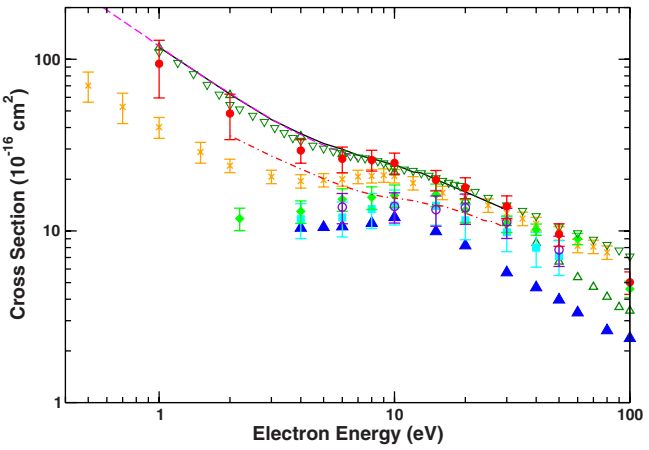

FIG. 4. (Color online) Integral elastic cross sections (ICS) and total scattering cross sections (TCS) for low-energy electron collisions with H_2O. ICS measurements: (●) (red), present, obtained with Born-dipole extrapolation to 0° at 20 eV and below and 4.6 meV inelasticity assumed; (▲) (blue), Danjo and Nishimura [13]; (♦) (green), Shyn and Cho [15] to 20 eV and Shyn and Grafe [17] at 30 eV and above; (○) (violet), Johnstone and Newell [16]; (■) (cyan), Cho *et al.* [18]; (△) (green), recommended ICS of Itikawa and Mason [1]. ICS calculations: (solid line) (black), present, with 10 meV inelasticity assumed; (dot-dashed line) (red), Varella *et al.* [30]; (dashed line) (magenta), rotationally summed result of Faure *et al.* [37]. TCS measurements: (▽) (green), recommended values of Itikawa and Mason [1], based on data of Kimura *et al.* [5] and Zecca *et al.* [8]; (×) (orange), Szmytkowski [3].

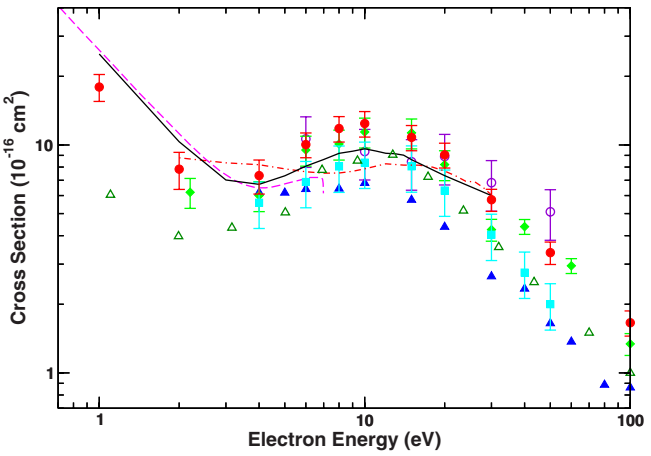

FIG. 5. (Color online) Momentum-transfer cross sections for low-energy electron collisions with H_2O. Experiments: (●) (red), present; (▲) (blue), Danjo and Nishimura [13]; (♦) (green), Shyn and Cho [15] to 20 eV and Shyn and Grafe [17] at 30 eV and above; (○) (violet), Johnstone and Newell [16]; (■) (cyan), Cho *et al.* [18]. Calculations: (solid line) (black), present; (dot-dashed line) (red), Varella *et al.* [30]; (dashed line) (magenta), Faure *et al.* [37]. (△) (green), recommended values of Itikawa and Mason [1].

large and small θ. To determine the extrapolation errors, we also flat-extrapolated the DCS towards small and large θ, using our DCS values at the smallest and largest θ measured, and have incorporated these errors into our ICS. We obtained an ICS from our calculated DCS by using an inelasticity of 10 meV in computing the dipole-Born correction. This value is arbitrary, but roughly comparable to the energies of typical allowed transitions among low-J levels that will be populated around room temperature; using a larger (smaller) inelasticity would produce a smaller (larger) ICS. As noted by Itikawa and Mason [63,66] and also applied in Kimura *et al.* [5], accounting for the forward scattering due to the dipole enhances the low-energy ICS by about a factor of 2. Indeed, we find that a "regular" extrapolation of our measured DCSs to zero angle would give an ICS at 1 eV of 41.4 ± 8.2 cm^2, while including the Born-dipole forward peak raises this to 94.2 ± 23.8 cm^2. We observe excellent agreement at 1 eV with the recommended ICS of Itikawa and Mason [1], but as E_0 exceeds 20 eV, their ICS begins to fall significantly below ours, by as much as 30% at 100 eV. We also note that if we did not use the Born-dipole extrapolation, our ICS would nicely match the TCS of Szmytkowski *et al.* [3,10] at low E_0, within error bars, suggesting that they may not have accounted for the Born-dipole DCS form in their forward scattering to correct their TCS. At higher E_0, the difference of about 18% between our ICS and the TCS of Szmytkowski *et al.* [3,10] can be adequately accounted for by the electronic [67], vibrational excitation (present experimental observations, to be published), and ionization [68] cross sections, which contribute about 2%, 4%, and 12% respectively. The present calculated ICS (assuming an inelasticity of 10 meV when making the Born-dipole correction) is very close to the rotationally summed ICS of Faure *et al.* [37] at the energies where they overlap and also generally agrees well with the present measured ICS.

Because the derivation of an ICS from measured or calculated DCSs is, for polar molecules such as H_2O, sensitive to assumptions made about the scattering at extreme forward angles, it is also instructive to examine the momentum transfer cross section (MTCS), which, due to its $(1-\cos\theta)$ weighting, is determined mostly by scattering at high and intermediate angles. In Fig. 5, we compare our measured and calculated MTCSs to each other and to literature values. Our calculated MTCS agrees well with that of Faure *et al.* [37] up to 4 eV, above which it becomes somewhat larger. From 4 to 20 eV, it agrees in shape with the MTCSs of Shyn and Cho [15] and of Cho *et al.* [18]. It is also generally consistent in magnitude with those MTCSs, within their respective error bars, as well as with the MTCS of Johnstone and Newell [16]. However, the MTCS of Danjo and Nishimura [13] and the recommended MTCS of Itikawa and Mason [1] are generally smaller than ours.

As a further check of our measured DCSs, in Fig. 6, we compare our measured DCSs at θ=90° with the relative DCSs of Seng and Linder [11], who in 1974 took very careful relative "excitation function" measurements of vibrationally elastic electron scattering from H_2O for E_0 from 1 eV to 10 eV over a finer grid of E_0 than ours. We have compared their relative DCSs to ours by normalizing at the peak, E_0=8 eV (arrow in Fig. 6). We note that the agreement between the two data sets is excellent. Further, about 6 months later, we repeated the excitation-function measurement over a finer grid than theirs, also using He for calibration, and once again observe excellent agreement with their results and our previously measured DCSs. This level of con-

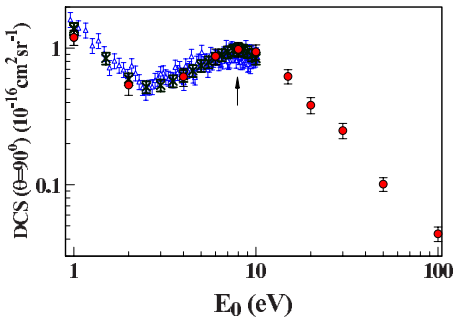

FIG. 6. (Color online) Comparison of the present (●) (red) elastic scattering DCSs at $\theta=90°$ with the relative (excitation function) DCSs of Seng and Linder [11] (×), normalized to present DCSs at $E_0=8$ eV (arrow); (△) (blue), later elastic scattering (excitation function) measurement taken by us at fixed θ of 90°. See text for discussion.

firmation is very encouraging. Indeed, Fig. 6 shows a smooth trend of our DCSs from 1 eV to 100 eV, a very large range. We also note the increase in the ICSs at E_0 around 10 eV, possibly due to a broad shape resonance.

IV. CONCLUSIONS

We have reported experimental DCSs for vibrationally elastic scattering of low- to intermediate-energy electrons from H_2O, as well as elastic DCSs calculated using the SMC method within the fixed-nuclei approximation. We find that our measured DCSs are higher than existing measurements, by about 30%–50%, but in excellent qualitative agreement with those measurements. Our measured DCSs are expected to be improvements over previous results because our technique does not rely, as in the conventional relative flow method, on a knowledge of molecular diameters of the gaseous targets. On the other hand, the present calculations are rather extensive and expected to be reliable, yet the DCSs they produce are, on the whole, smaller than the present measured DCSs and in good general agreement with previous measurements and calculations. We presently have no explanation for the discrepancy. Finally, both our measured and our calculated ICSs are in excellent agreement with the recommended ICSs of Itikawa and Mason [1] for low E_0 values, but for E_0 values higher than 20 eV, the recommended ICSs fall significantly below ours.

ACKNOWLEDGMENTS

This work was sponsored by the U.S. National Science Foundation through Grants No. PHY-0653452 and No. PHY-0653396 and by the Brazilian Conselho Nacional de Desenvolvimento Cientifico e Tecnológico (CNPq) under a collaborative program. We acknowledge important discussions with Dr. Yukikazu Itikawa (Institute of Space and Aeronautical Science, Japan) and Dr. Fu-Ming Tao (California State University, Fullerton, USA). We thank Dr. M. H. F. Bettega (Universidade Federal do Paraná, Brazil) for sending us tabulated elastic scattering DCSs of Refs. [30,31]. Work by C.W. and V.M. was also supported by the Chemical Sciences, Biosciences, and Geosciences Division, Office of Basic Energy Science, Office of Science, U.S. Department of Energy, and made use of the Jet Propulsion Laboratory's Supercomputing and Visualization Facility. M.C.A.L. and H.S. acknowledge support from CNPq, from Coordenação de Aperfeiçoamento de Pessoal de Nível Superior (CAPES), and from Fundação de Amparo à Pesquisa do Estado de Minas Gerais (FAPEMIG).

[1] Y. Itikawa and N. Mason, J. Phys. Chem. Ref. Data **34**, 1 (2005).
[2] S. M. Pimblott and L. D. A. Siebbeles, Nucl. Instrum. Methods Phys. Res. B **194**, 237 (2002).
[3] C. Szmytkowski, Chem. Phys. Lett. **136**, 363 (1987).
[4] O. Sueoka, S. Mori, and Y. Katayama, J. Phys. B **19**, L373 (1986).
[5] M. Kimura, O. Sueoka, A. Hamada, and Y. Itikawa, Adv. Chem. Phys. **111**, 537 (2000).
[6] Z. Sağlam and N. Aktekin, J. Phys. B **23**, 1529 (1990).
[7] H. Nishimura and K. Yano, J. Phys. Soc. Jpn. **57**, 1951 (1988).
[8] A. Zecca, G. Karwasz, S. Oss, R. Grisenti, and R. S. Brusa, J. Phys. B **20**, L133 (1987).
[9] C. Szmytkowski and P. Możejko, Opt. Appl. **36**, 543 (2006).
[10] C. Szmytkowski, K. Maciąg, P. Koenig, A. Zecca, S. Oss, and R. Grisenti, Chem. Phys. Lett. **179**, 114 (1991).
[11] G. Seng and F. Linder, J. Phys. B **7**, L509 (1974).
[12] K. Jung, T. Antoni, R. Muller, K.-H. Kochem, and H. Ehrhardt, J. Phys. B **15**, 3535 (1982).
[13] A. Danjo and H. Nishimura, J. Phys. Soc. Jpn. **54**, 1224 (1985).
[14] A. Katase, K. Ishibashi, Y. Matsumoto, T. Sakae, S. Maezono, E. Murakami, K. Watanabe, and H. Maki, J. Phys. B **19**, 2715 (1986).
[15] T. W. Shyn and S. Y. Cho, Phys. Rev. A **36**, 5138 (1987).
[16] W. M. Johnstone and W. R. Newell, J. Phys. B **24**, 3633 (1991).
[17] T. Shyn and A. Grafe, Phys. Rev. A **46**, 4406 (1992).
[18] H. Cho, Y. S. Park, H. Tanaka, and S. J. Buckman, J. Phys. B **37**, 625 (2004).
[19] S. K. Srivastava, A. Chutjian, and S. Trajmar, J. Chem. Phys. **63**, 2659 (1975).
[20] F. H. Read and J. M. Channing, Rev. Sci. Instrum. **67**, 2372 (1996).
[21] F. A. Gianturco and D. G. Thompson, J. Phys. B **13**, 613 (1980).
[22] A. Jain and D. G. Thompson, J. Phys. B **15**, L631 (1982).
[23] L. M. Brescansin, M. A. P. Lima, T. L. Gibson, V. McKoy, and W. M. Huo, J. Chem. Phys. **85**, 1854 (1986).
[24] F. A. Gianturco and S. Scialla, J. Chem. Phys. **87**, 6468 (1987).
[25] T. N. Rescigno and B. H. Lengsfield, Z. Phys. D: At., Mol. Clusters **24**, 117 (1992).
[26] Y. Okamoto, K. Onda, and Y. Itikawa, J. Phys. B **26**, 745

(1993).
[27] R. Greer and D. Thompson, J. Phys. B **27**, 3533 (1994).
[28] L. E. Machado, L. Mu-Tao, L. M. Brescansin, M. A. P. Lima, and V. McKoy, J. Phys. B **28**, 467 (1995).
[29] F. A. Gianturco, S. Meloni, P. Paioletti, R. R. Lucchese, and N. Sanna, J. Chem. Phys. **108**, 4002 (1998).
[30] M. T. do N. Varella, M. H. F. Bettega, M. A. P. Lima, and L. G. Ferreira, J. Chem. Phys. **111**, 6396 (1999).
[31] A. P. P. Natalense, M. T. do N. Varella, M. H. F. Bettega, L. G. Ferreira, and M. A. P. Lima, Braz. J. Phys. **31**, 15 (2001).
[32] H. Aouchiche, C. Champion, and D. Oubaziz, Radiat. Phys. Chem. **77**, 107 (2008).
[33] L. Caron, D. Bouchiha, J. D. Gorfinkiel, and L. Sanche, Phys. Rev. A **76**, 032716 (2007).
[34] D. Bouchiha, L. G. Caron, J. D. Gorfinkiel, and L. Sanche, J. Phys. B **41**, 045204 (2008).
[35] A. Muñoz, J. C. Oller, F. Blanco, J. D. Gorfinkiel, P. Limão-Vieira, and G. Garcia, Phys. Rev. A **76**, 052707 (2007).
[36] A. Muñoz, F. Blanco, G. Garcia, P. A. Thorn, M. J. Brunger, J. P. Sullivan, and S. J. Buckman, Int. J. Mass. Spectrom. **277**, 175 (2008).
[37] A. Faure, J. D. Gorfinkiel, and J. Tennyson, J. Phys. B **37**, 801 (2004).
[38] A. Faure, J. D. Gorfinkiel, and J. Tennyson, Mon. Not. R. Astron. Soc. **347**, 323 (2004).
[39] K. Takatsuka and V. McKoy, Phys. Rev. A **24**, 2473 (1981); **30**, 1734 (1984).
[40] H. Silva, J. Muse, M. C. A. Lopes, and M. A. Khakoo, Phys. Rev. Lett. **101**, 033201 (2008).
[41] M. J. Brunger and S. J. Buckman, Phys. Rep. **357**, 215 (2002).
[42] M. A. Khakoo, K. Keane, C. Campbell, N. Guzman, and K. Hazlett, J. Phys. B **40**, 3601 (2007).
[43] F. Rugamas, D. Roundy, G. Mikaelian, G. Vitug, M. Rudner, J. Shih, D. Smith, J. Segura, and M. A. Khakoo, Meas. Sci. Technol. **11**, 1750 (2000).
[44] S. Dushman, *Vacuum Technique* (Wiley, New York, 1949), pp. 36 and 43.
[45] N. Goldman, C. Leforestier, and R. J. Saykally, J. Phys. Chem. A **108**, 787 (2004).
[46] M. A. Khakoo, C. E. Beckmann, S. Trajmar, and G. Csanak, J. Phys. B **27**, 3159 (1994).
[47] ARi Industries Inc., 381 ARi Court, Addison, Illinois 60101, BXX06B41-4K heater.
[48] EPT AF150 Equipe Thermodynamique et Plasmas (ETP) model AF151.
[49] J. H. Brunt, G. C. King, and F. H. Read, J. Phys. B **10**, 1289 (1977).
[50] M. Hughes, K. E. James, Jr., J. G. Childers, and M. A. Khakoo, Meas. Sci. Technol. **14**, 841 (1994).
[51] J. Muse, H. Silva, M. C. A. Lopes, and M. A. Khakoo, J. Phys. B **41**, 095203 (2008).
[52] M. A. Khakoo, J. Blumer, K. Keane, C. Campbell, H. Silva, M. C. A. Lopes, C. Winstead, V. McKoy, R. F. da Costa, L. G. Ferreira, M. A. P. Lima, and M. H. F. Bettega, Phys. Rev. A **77**, 042705 (2008).
[53] R. K. Nesbet, Phys. Rev. A **20**, 58 (1979).
[54] D. F. Register, S. Trajmar, and S. K. Srivastava, Phys. Rev. A **21**, 1134 (1980).
[55] C. Winstead and V. McKoy, Comput. Phys. Commun. **128**, 386 (2000).
[56] M. W. Schmidt, K. K. Baldridge, J. A. Boatz, S. T. Elbert, M. S. Gordon, J. H. Jensen, S. Koseki, N. Matsunaga, K. A. Nguyen, S. J. Su, T. L. Windus, M. Dupuis, and J. A. Montgomery, J. Comput. Chem. **14**, 1347 (1993).
[57] T. H. Dunning, Jr., J. Chem. Phys. **90**, 1007 (1989).
[58] R. A. Kendall, T. H. Dunning, Jr., and R. J. Harrison, J. Chem. Phys. **96**, 6796 (1992).
[59] C. W. Bauschlicher, J. Chem. Phys. **72**, 880 (1980).
[60] T. N. Rescigno and B. I. Schneider, Phys. Rev. A **45**, 2894 (1992), and references therein.
[61] F. A. Gianturco and A. Jain, Phys. Rep. **143**, 347 (1986).
[62] S. L. Shostak, W. L. Ebenstein, and J. S. Muenter, J. Chem. Phys. **94**, 5875 (1991).
[63] J. Tennyson, N. F. Zobov, R. Williamson, O. L. Polyansky, and P. F. Bernath, J. Phys. Chem. Ref. Data **30**, 735 (2001).
[64] M. A. Khakoo, J. Muse, H. Silva, M. C. A. Lopes, C. Winstead, V. McKoy, E. M. de Oliveira, R. F. da Costa, M. T. do N. Varella, M. H. F. Bettega, and M. A. P. Lima (unpublished).
[65] R. D. Nelson, Jr., D. R. Lide, Jr., and A. A. Maryott, http://www.nist.gov/srd/nsrds.htm.
[66] Y. Itikawa (private communication).
[67] P. A. Thorn, M. J. Brunger, H. Kato, M. Hoshino, and H. Tanaka, J. Phys. B **40**, 697 (2007).
[68] Y.-K. Kim and M. E. Rudd, Phys. Rev. A **50**, 3954 (1994).